The International Journal of Advanced Manufacturing Technology (2018) 98:2231–2237
https://doi.org/10.1007/s00170-018-2377-z

ORIGINAL ARTICLE

# Properties of injection-molded poly (L-co-D,L-lactic acid) using different melt temperatures and stress concentrator in the specimen geometry

G. V. Salmoria[1,2] · L. F. Vieira[1,2] · I. M. Gindri[2] · C. R. M. Roesler[2] · E. A. Fancello[2,3]

Received: 19 April 2018 / Accepted: 25 June 2018 / Published online: 3 July 2018


## Abstract

This paper investigates the morphology and mechanical properties of poly (L-co-D,L-lactic acid) (PLDLA) specimens injection-molded using different melt temperatures and stress concentrator in the specimen geometry. The values for the tensile strength and ultimate strain increased with a reduction in the melt injection temperature for unnotched specimens. The notched specimens molded using low and high melt injection temperatures showed similar values for the tensile strength compared with the unnotched specimens. The fracture surfaces of the notched and unnotched specimens molded at the low melt temperature showed the characteristic of ductile failure presenting fibrillation and displacement in the oriented skin layer. A restriction in the chain rotation and conformation due to the oriented skin layer explains the less viscous behavior observed in the dynamic mechanical analysis for low injection temperature specimens. The photoelastic analysis indicated a birefringence along the specimens manufactured using the low melt injection temperature, suggesting the existence of residual stress due to filling phase and rapid solidification. On the other hand, specimens injected using the high temperature showed residual stress concentration near the gate due to the packing effect of holding pressure. The enthalpic relaxation peak at the glass transition ($T_g$) observed in the differential scanning calorimetry analysis confirmed the existence of significant residual stress in all PLDLA specimens, especially when injected using the low temperature.

**Keywords** Poly (L-co-D,L-lactic acid) · Injection molding · Effect of processing conditions

✉ G. V. Salmoria
gean.salmoria@ufsc.br

L. F. Vieira
luizfernandovieira@posgrad.ufsc.br

I. M. Gindri
izabellegindri@hotmail.com

C. R. M. Roesler
r.roesler@ufsc.br

E. A. Fancello
Eduardo.fancello@ufsc.br

[1] CIMJECT Laboratory, Department of Mechanical Engineering, Federal University of Santa Catarina, Florianópolis, SC 88040-900, Brazil

[2] Biomechanics Engineering Laboratory, University Hospital (HU), Federal University of Santa Catarina, Florianópolis, SC 88040-900, Brazil

[3] GRANTE, Department of Mechanical Engineering, Federal University of Santa Catarina, Florianópolis, SC 88040-900, Brazil

## 1 Introduction

Injection molding processes are used to produce medical devices comprised of bioabsorbable polymers, such as poly (lactic acid) (PLA), which are absorbed by the body over a controlled period of time. Current applications of PLA polymers include dental scaffolds, maxillofacial plates, orthopedic screws, ligament anchors, nerve regeneration guides, and vascular drug-eluting stents [1–5]. Many of these products are small, complex, 3D geometries that can only be manufactured using injection molding. Specialists are working toward obtaining better control of the bioabsorbable polymer morphology and properties during processing, in order to expand the possibilities for manufacturing medical devices with complex geometries [6, 7].

The properties of an injection-molded part are strongly influenced by the polymer morphological features, such as the crystallinity and molecular orientation [5, 8]. The polymer morphology varies according to the complex thermal and mechanical history of the material associated

with the molding process and is known to vary depending on the location within a molded part as well as on the injection conditions, which can result in an anisotropic morphology and residual stress [9, 10]. Molecular orientation usually occurs close to the surface due to the elongational flow at the flow front. The orientation in the subskin layer (or close to the core of the part) is related to the shear flow and it can influence the semicrystalline and amorphous properties of the polymer [11–13].

PLA exists in two optical stereo-isomeric forms: poly (L-lactic acid), PLLA, and poly (D-lactic acid), PDLA. Optically pure PLLA and PDLA are semicrystalline polymers, while the racemic PLDLA is amorphous and it is used in a number of medical devices [7]. Crystallinity results in slower degradation rate, which has been associated with in vivo inflammatory reaction. Furthermore, PLLA is a brittle material with the potential to accumulate residual stress [1, 3, 6, 8, 14]. In an attempt to overcome PLLA limitations, a combination of L-lactic and D,L-lactic monomers resulting in a poly (L-co-D,L-lactic acid) (PLDLA) copolymer has been studied. PLDLA has presented a better degradation rate in comparison to PLLA and good mechanical properties. However, the latter is strongly affected by the processing conditions and part geometry. In order to establish relationships between the mechanical properties and the processing parameters, part geometry, and PLDLA morphological features, it is desirable to optimize the mechanical behavior of the molded PLDLA. This paper describes a study on the morphology and mechanical properties of PLDLA injection-molded specimens using different melt temperatures and stress concentrator in the specimen geometry.

## 2 Experimental

### 2.1 Materials

The material used in this study was Purasorb 7038, a PLDLA (poly(L-lactide-co-D,L-lactide) 70:30) supplied by PURAC Biochem (Gorinchem, The Netherlands). The PLDLA was estimated by the supplier to have a D-lactide content of 15%. The Mn value was 300,000 g/mol and the polydispersity was 1.4, as determined by gel permeation chromatography (Shimadzu LC, 10A, Japan) at 31 °C in THF with p-Styragel 106, 105, 104, and 103 columns and a polystyrene standard.

### 2.2 Injection molding

Previously prepared pellets were dried in an air circulating oven at 50 °C for 24 h to remove the moisture. Dried pellets were then fed into an Arburg Allrounder 270S 250-70 injection molding machine, and two different geometries (notched and unnotched) of tensile specimens (62 mm × 16 mm × 2.0 mm) with a dumbbell shape were obtained, with the smallest rectangular cross section being 10 mm × 2.0 mm, adapted from ASTM D1822 type S and ASTM D638 type V specimens.

The geometries of the two mold cavities are shown in Fig. 1. A notched specimen, with a stress concentration factor of 2.4, was investigated, aimed at mimicking the complex geometry corners commonly found in medical devices such as screws and anchors.

The injection molding conditions investigated in this study were as follows: injection flow rate 25 $cm^3$/s, mold temperature 25 °C, holding pressure 60 MPa (600 bar), holding time 9 s, injection time 2 s, cooling time 50 s, and screw speed 100 rpm. The melt injection temperature and the part geometry were chosen as the investigated variables. Two melt injection temperatures ($T_m$) were considered: 205 and 235 °C. The geometry is represented by the notched and unnotched specimens. The other process parameters were set considering the machine limits, melt viscosities, and mold filling characteristics. The factorial design for this study is shown in Table 1. Three samples were prepared for each condition.

### 2.3 Morphology characterization and fractography

A Reichert Jung SN microtome equipped with a steel knife was used to obtain 30 μm cross sections of the central part of molded specimens. The temperature was kept at 20 °C to reduce the extent of surface deformation. The speed of the knife was 1 mm/s. The morphology of the cut cross sections was observed using a Leica DM LM transmission microscope.

The fracture surfaces of the tensile test PLDLA specimens were examined using a JEOL JSM-6390LV scanning electron microscope (SEM). The specimens were coated with a thin layer of gold using a sputter coater diode D2 sputtering system.

### 2.4 Tensile tests and dynamic mechanical analysis

The specimens were tested on an EMIC DL-3000 universal testing machine. A minimum number of five specimens from each processing condition were tested. These tests were performed at a controlled room temperature of 23 °C and at a test velocity of 1.0 mm/min.

A DMA Q800 analyzer (TA Instruments) with a single cantilever clamp was used to perform a dynamic mechanical analysis (DMA). This test provided the values for the storage modulus (*E*'), loss modulus (*E*"), and tan delta ($\delta$) at a frequency of 1 Hz within the temperature range of − 10 to 120 °C using a heating rate of 3 °C/min and strain of 0.3%.

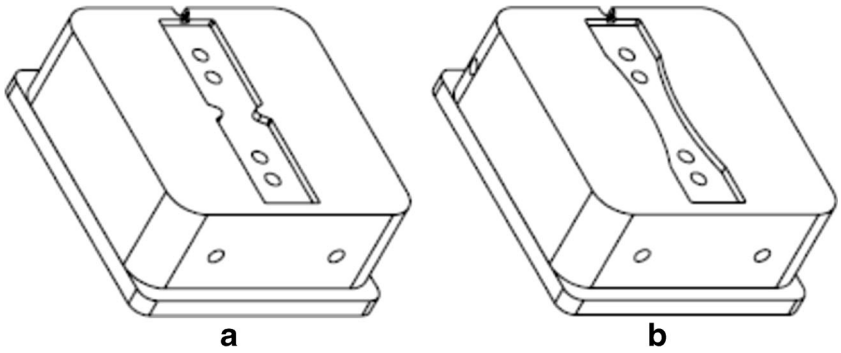


**Fig. 1** Illustration of the mold cavities used for the injection molding of the two different geometries. Notched specimen (**a**) and regular unnotched specimen (**b**)

### 2.5 Photoelastic analysis and differential scanning calorimetry

The residual stress of molded specimens was investigated by photoelasticity isochromatic fringes [15]. A polariscope was used to capture the birefringence of the molded specimens and convert it into fringes. The number of fringes is proportional to the optical anisotropy due to residual stress.

To determine the residual stress by thermal analysis, differential scanning calorimetry was performed on 10 mg samples taken from the central region of molded specimens, using a Shimadzu DSC-50, applying a heating rate of 10 °C/min and nitrogen flow rate of 50 ml/min.

## 3 Results and discussion

Stress versus strain curves for the four conditions of the factorial study is shown in Fig. 2. The unnotched (regular) specimens molded using the low and high melt injection temperatures presented almost the same average apparent elastic modulus, but higher values for the tensile strength and strain at break were observed in the former case. The average value for the apparent elastic modulus reduced from 2503 to 2481 MPa and the tensile strength reduced from 59 to 52 MPa (Table 2) with the increase in temperature. The notched specimens molded using the low and high melt injection temperatures presented almost the same average apparent elastic modulus, tensile strength, and strain at break (Table 2).

Figure 2 also shows the images of the lateral view of the tested specimens. A small reduction can be observed in the cross-sectional area of the specimens molded using the low injection temperature, unnotched–low $T_m$ and notched–low $T_m$, with withering and flow marks. This behavior may be explained based on the greater degree of local elongation achieved (strain at break of 8%). Conversely, the specimens molded using the high injection temperature show a brittle behavior, i.e., without apparent local plastic strains. Similar effects of the melt injection temperature on the strength and strain at break have been reported for the injection molding of semicrystalline PLLA [7].

The micrographs of the fracture surfaces (Fig. 3) of notched and unnotched specimens molded using the low melt temperature show characteristic features of ductile failure, presenting significant plastic deformations, such as fibrillation and layer displacement, especially in the external regions.

The difference between the deformation behaviors in the external regions and the core of the central portion of specimens (where the fracture was observed) is probably related to a heterogenic morphology generated during processing. As

**Table 1** Summary of the factorial design of the experiment

| Input variables | Number of levels | Levels |
|---|---|---|
| $T_m$—melt injection temperature | 2 | Low (205 °C)<br>High (235 °C) |
| Notch | 2 | Notched<br>Unnotched |

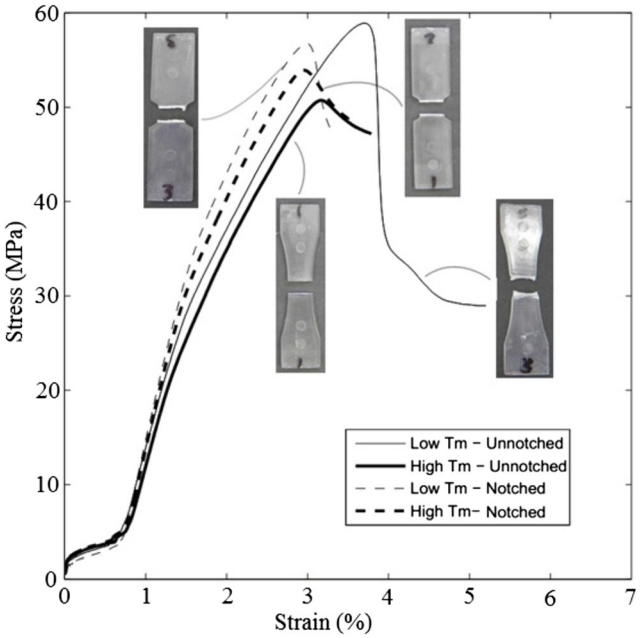


**Fig. 2** Tensile test curves for notched and unnotched specimens molded using the low and high injection temperatures ($T_m$)

**Table 2** Mechanical properties of PLDLA specimens determined from tensile tests

| Specimen | Elastic modulus (MPa) | Strength (MPa) | Strain at break (%) |
|---|---|---|---|
| Unnotched–low $T_m$ | 2503 (± 40) | 59 (± 2) | 8 (± 1.5) |
| Unnotched–high $T_m$ | 2481 (± 80) | 52 (± 2) | 3 (± 2.0) |
| Notched–low $T_m$ | 2910 (± 90) | 56 (± 3) | 3 (± 1.5) |
| Notched–high $T_m$ | 2867 (± 30) | 53 (± 2) | 3 (± 1.0) |

observed in Figs. 3 and 4, oriented skin and subskin layers and a non-oriented core were detected for all samples, but with different characteristics between them. The specimens molded using the low melt injection temperature (unnotched–low $T_m$ and notched–low $T_m$) tended to solidify with molecular orientation close to the mold wall, which is due to elongational flow.

The orientation in the subskin layer, as shown in Fig. 4, is related to the shear flow in PLAs and can also lead to solidification at high cooling rates observed in samples molded using the low melt injection temperature [6]. This behavior may explain the large plastic deformation with the dislocation of subskin layers, as observed on the fracture surface of unnotched–low $T_m$ and notched–low $T_m$ specimens. Oval- and square-shape structures were observed in the core region of unnotched–low $T_m$ and notched–low $T_m$ specimens, respectively, which were associated with different molecular orientation and mechanical behavior in the material's core and subskin regions (Fig. 3). The molecular orientation of the thicker skin layer in unnotched–low $T$ conferred to this region a greater characteristic of plastic deformation after fracture, as shown by the larger magnification in Fig. 3. These results were further supported by higher values for the apparent elastic modulus, tensile strength, and strain at break for unnotched–low $T$, as previously reported for PLLA injection molding [6, 7].

Notched and unnotched specimens molded with the high injection temperature presented flat and smooth fracture surfaces (Fig. 3), as typically found in brittle polymeric materials with high-speed flaw propagation during failure [16]. Small plastic deformations can be seen near the borders, suggesting the formation of a thin molecular-oriented skin layer during the elongational flow. There is no evidence of subskin layers, indicating the presence of an extended core region without orientation. These features suggest that for samples prepared at higher temperature, the cooling rate was slow enough to allow the relaxation of a significant portion of the specimen resulting in a non-oriented morphology and brittle mechanical behavior, similar to non-oriented injection-molded PLLA [7].

These observations are in agreement with the polarized optical microscopy images shown in Fig. 4 and the values obtained for the skin layer thickness reported in Table 3. A skin layer of about 70 μm was obtained for unnotched–low $T_m$ and notched–low $T_m$, while a skin layer thickness of around 10 μm was verified for unnotched–high $T_m$ and notched–high $T_m$. These characteristics can be explained by the processing conditions. During the injection molding process, the molten polymer is subjected to shear and elongational flow prior to

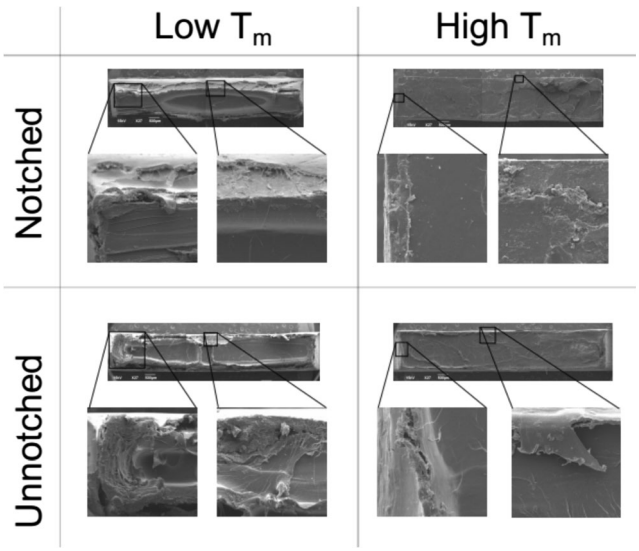


**Fig. 3** SEM micrographics of the fracture surface of notched and unnotched specimens molded using low and high melt injection temperatures ($T_m$). × 20 magnification

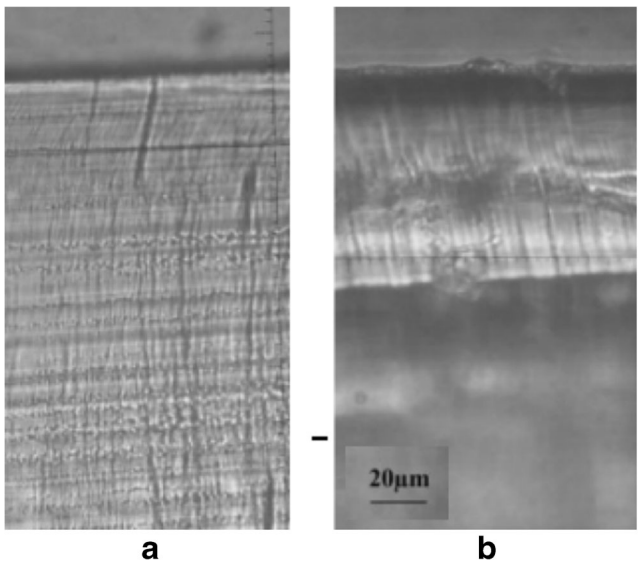


**Fig. 4** Optical micrographics of cross section of unnotched specimens. **a** Thin skin layer of specimen molded at the high injection temperature. **b** Thick skin layer of specimen molded at the low injection temperature

**Table 3** Skin layer thickness determined by polarized optical microscopy

| Sample | Skin layer thickness [μm] | |
|---|---|---|
| | Low $T_m$ | High $T_m$ |
| Unnotched | 74 (± 11) | 7 (± 3) |
| Notched | 69 (± 15) | 12 (± 4) |

solidification. Specimens molded with the same polymer may present considerably different morphologies depending on the processing conditions [17]. Typically, molecular orientation occurs when the flow and cooling rates are sufficiently fast. Therefore, samples processed at lower temperatures are observed to have a faster cooling hate than samples processed at higher temperatures. This explains the findings observed in this study in which unnotched–low $T_m$ and notched–low $T_m$ presented a thicker and organized skin layer, while high $T_m$ and notched–high $T_m$ present a discrete organized layer.

In DMA tests, a cyclic force is applied to the specimens at a specified frequency and the storage modulus ($E$'), loss modulus ($E$"), and loss tangent ($E$"/$E$') are measured as functions of the temperature, highlighting changes in the stiffness and damping characteristics. Specimens molded at the high injection temperature showed higher loss tangents than those molded at the low injection temperature, suggesting that the former has a greater number of molecular groups with the freedom to undergo rotation and conformation during the glass transition ($T_g$). In addition, the lower loss tangent values observed for the specimens molded at the low injection temperature are consistent with the presence of thick oriented skin layers, since strong molecular orientation introduces constraints in the molecular movement (Fig. 5).

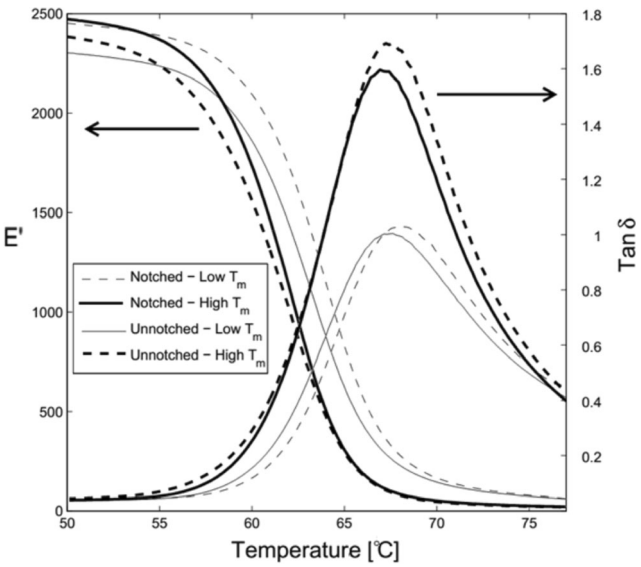


**Fig. 5** Storage modulus ($E$') and loss tangent (tan $\delta$) of notched–low $T$, notched–high $T$, unotched–low $T$, and unotched–high $T$

Photoelasticity allows the analysis of the residual stress distribution due to a heterogeneous cooling rate and mold overpacking. According to the Maxwell and Brewest laws, the birefringence of a material presenting optical anisotropy ($n_{11}$–$n_{22}$) can be related directly to the difference in the corresponding principal stresses, that is, $\tau_{11}$–$\tau_{22}$, for a light propagated along one of the principal axes of the strain:

$$(n_{11}–n_{22}) = C\,(\tau_{11}–\tau_{22}) \quad (1)$$

where $C$ is the stress-optical coefficient, which is dependent on the temperature and the polymer chain refraction index (electronic polarizability). The photoelastic effect, characterized by the stress-optical coefficient, is primarily determined by the anisotropic polarizability [18]. Figure 6 shows the photoelastic fringes of notched and unnotched specimens injected at low and high temperatures. Both low injection temperature specimens (a and c) show fringes that suggest a wide distribution of residual stresses, probably due to the shear stress during the filling phase and the rapid solidification. On the other hand, the high injection temperature specimens (b and d) present residual stresses concentrated at the gate and in the central regions due to the packing effect of holding pressure.

Figure 7 shows the results obtained in the differential scanning calorimetry (DSC) analysis. Curve A shows the thermal behavior of annealed (amorphous) pellets of PLDLA, where a single glass transition at 59 °C is observed from the pronounced step in the baseline curve due to a change in the heating capacity ($C_p$). On the other hand, analogous curves of injected specimens showed clear endothermic peaks at the same temperature of 59 °C which are attributed to the residual stresses induced during the molding process [19]. The energy involved in the enthalpic relaxation peaks of the specimens molded using the low injection temperature was higher than that for the specimens molded with the high injection temperature (Table 4). This suggests that the low injection temperature molding process produced higher residual stresses, at least in the central region.

## 4 Conclusions

Temperature and geometry were observed to be an important factor on the manufacturing process of PLDLA samples. Lower temperature resulted in higher tensile strength and ultimate strain for unnotched specimens, which were associated with formation of skin and subskin organized layers on these samples. The notched specimens molded using low and high melt injection temperatures showed similar values for the tensile strength compared with the

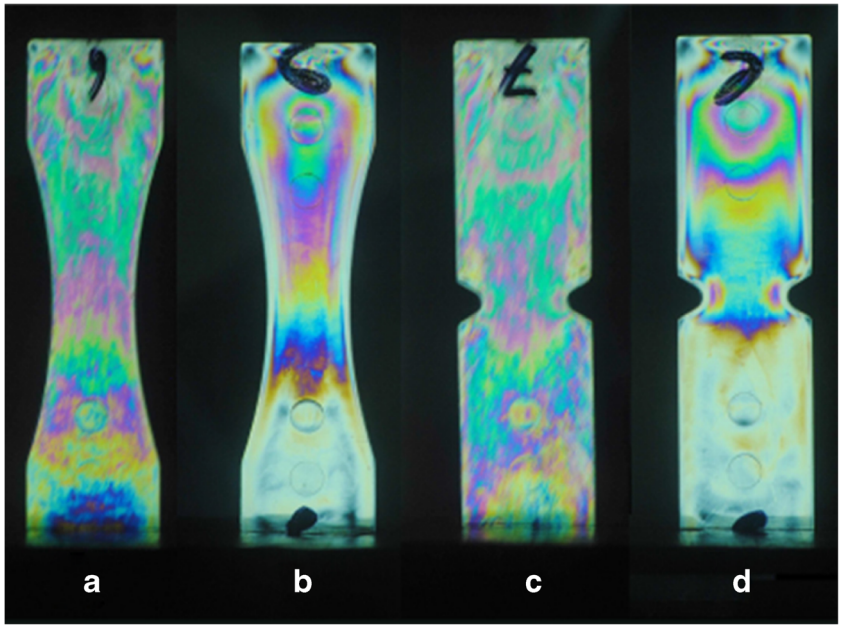


**Fig. 6** Images of photoelastic fringes for **a** notched–low *T*, **b** notched–high *T*, **c** unotched–low *T*, and **d** unotched–high *T*

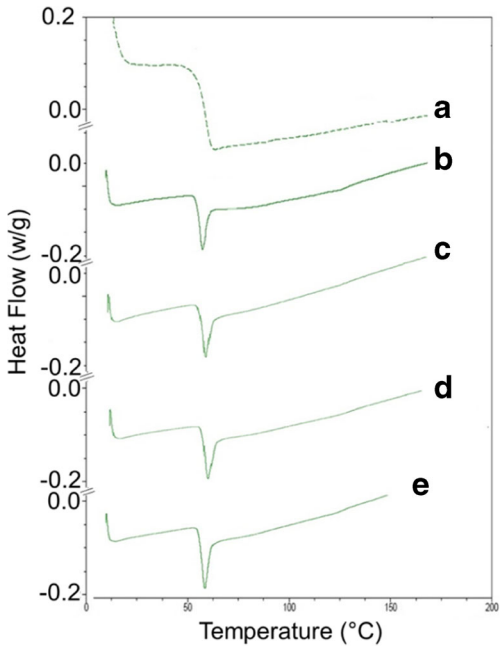


**Fig. 7** Calorimetry curves for **a** annealed PLDLA pellets, **b** notched–low *T*, **c** notched–high *T*, **d** unotched–low *T*, and **e** unotched–high *T*

**Table 4** Relaxation enthalpy values for PLDLA specimens determined by DSC

| PLDLA specimens | Low $T_m$ (J/g) | High $T_m$ (J/g) |
|---|---|---|
| Unnotched | 6.9 (± 0.9) | 5.6 (± 0.8) |
| Notched | 7.2 (± 0.9) | 5.2 (± 0.8) |

unnotched specimens. Specimens molded using the low melt injection temperature presented lower loss tangent values in the DMA tests. Molecular restriction in the chain rotation and conformation due to the thick oriented skin layer can explain the less viscous behavior observed in the DMA for notched and unnotched low injection temperature specimens. The photoelastic analysis indicated a birefringence along the specimens manufactured using the low melt injection temperature, suggesting an extended residual stress due to rapid solidification. On the other hand, specimens injected using the high temperature showed residual stress concentration at the gate region due to the compression effect of the holding pressure. The enthalpic relaxation peak at the $T_g$ observed in the DSC analysis confirmed the existence of significant residual stress in all PLDLA specimens, especially when injected using the low temperature. The results found in this work demonstrated the influence of processing parameters on materials properties, highlighting the importance in selecting the proper experimental conditions to manufacture samples with required properties. Effects of other parameter processes, such as injection pressure, will be evaluated in future works.

**Acknowledgements** The authors would like to thank the Center of Microscopy-UFSC for providing the micrographs.

**Funding information** The study was financially supported by PRONEX/FAPESC, CNPQ, CAPES, and FINEP.

## References


1. Södergård A, Stolt M (2002) Properties of lactic acid based polymers and their correlation with composition. Prog Polym Sci 27: 1123–1163. https://doi.org/10.1016/S0079-6700(02)00012-6
2. Gilding DK, Reed AM (1979) Biodegradable polymers for use in surgery—polyglycolic/poly(actic acid) homo- and copolymers: 1. Polymer (Guildf) 20:1459–1464. https://doi.org/10.1016/0032-3861(79)90009-0
3. Middleton JC, Tipton AJ (2000) Synthetic biodegradable polymers as orthopedic devices. Biomaterials 21:2335–2346. https://doi.org/10.1016/S0142-9612(00)00101-0
4. Salmoria GV, Klauss P, Paggi RA, Kanis LA, Lago A (2009) Structure and mechanical properties of cellulose based scaffolds fabricated by selective laser sintering. Polym Test 28:648–652. https://doi.org/10.1016/j.polymertesting.2009.05.008
5. Eberhart RC, Su S-H, Nguyen KT, Zilberman M, Tang L, Nelson KD, Frenkel P (2003) Bioresorbable polymeric stents: current status and future promise. J Biomater Sci Polym Ed 14:299–312
6. Ghosh S, Viana JC, Reis RL, Mano JF (2008) Bi-layered constructs based on poly(L-lactic acid) and starch for tissue engineering of osteochondral defects. Mater Sci Eng C 28:80–86. https://doi.org/10.1016/J.MSEC.2006.12.012
7. Ghosh S, Viana JC, Reis RL, Mano JF (2007) Effect of processing conditions on morphology and mechanical properties of injection-molded poly(L-lactic acid). Polym Eng Sci 47:1141–1147. https://doi.org/10.1002/pen.20799
8. Lim L-T, Auras R, Rubino M (2008) Processing technologies for poly(lactic acid). Prog Polym Sci 33:820–852. https://doi.org/10.1016/J.PROGPOLYMSCI.2008.05.004
9. Wagner AH, Yu JS, Kalyon DM (1989) Microstructure and ultimate properties of injection molded amorphous engineering plastics: poly(ether imide) and poly(2,6-dimethyl-1,4-phenylene ether). Polym Eng Sci 29:1298–1307. https://doi.org/10.1002/pen.760291813
10. Son Y, Hyun Ahn K, Char K Morphology of injection molded modified poly(pheny1ene oxide)/polyamide-6 blends
11. Azimi M, Mirjavadi SS, Hamouda AMS, Makki H (2017) Heterogeneities in polymer structural and dynamic properties in graphene and graphene oxide nanocomposites: molecular dynamics simulations. Macromol Theory Simulations 26:1600086. https://doi.org/10.1002/mats.201600086
12. Hoseinlaghab S, Mirjavadi SS, Sadeghian N, Jalili I, Azarbarmas M, Besharati Givi MK (2015) Influences of welding parameters on the quality and creep properties of friction stir welded polyethylene plates. Mater Des 67:369–378. https://doi.org/10.1016/J.MATDES.2014.11.039
13. Viana JC, Cunha AM, Billon N (2002) The thermomechanical environment and the microstructure of an injection moulded polypropylene copolymer. Polymer (Guildf) 43:4185–4196. https://doi.org/10.1016/S0032-3861(02)00253-7
14. Smit TH, Engels TAP, Söntjens SHM, Govaert LE (2010) Time-dependent failure in load-bearing polymers: a potential hazard in structural applications of polylactides. J Mater Sci Mater Med 21: 871–878. https://doi.org/10.1007/s10856-009-3921-z
15. American Society for Testing and Materials (214AD) ASTM D 4093 - Standard test method for photoelastic measurements of birefringence and residual strains in transparent or translucent plastic materials. https://compass.astm.org/EDIT/html_annot.cgi?D4093+95(2014). Accessed 6 Jun 2018
16. Salmoria GV, Ahrens CH, Fredel M, Soldi V, Pires ATN (2005) Stereolithography somos 7110 resin: mechanical behavior and fractography of parts post-cured by different methods. Polym Test 24:157–162. https://doi.org/10.1016/J.POLYMERTESTING.2004.09.008
17. Daly ' H Ben, Sanschagrin ' B, Clrcl KTN, Cole2 KC Effect of polymer properties on the structure of injection-molded parts
18. B. A. G. Schrauwen, L. C. A. v. Breemen, A. B. Spoelstra, L. E. Govaert, G. W. M. Peters, H. E. H. Meijer (2004) Structure, deformation, and failure of flow-oriented semicrystalline polymers. doi: https://doi.org/10.1021/MA048884K, 37, 8618, 8633
19. Pietrzak WS (2007) Rapid cooling through the glass transition transiently increases ductility of PGA/PLLA copolymers: a proposed mechanism and implications for devices. J Mater Sci Mater Med 18:1753–1763. https://doi.org/10.1007/s10856-007-3047-0